Since January 2020 Elsevier has created a COVID-19 resource centre with free information in English and Mandarin on the novel coronavirus COVID-19. The COVID-19 resource centre is hosted on Elsevier Connect, the company's public news and information website.

Journal of Quantitative Spectroscopy & Radiative Transfer 262 (2021) 107489

Contents lists available at ScienceDirect

Journal of Quantitative Spectroscopy & Radiative Transfer

journal homepage: www.elsevier.com/locate/jqsrt

Viruses such as SARS-CoV-2 can be partially shielded from UV radiation when in particles generated by sneezing or coughing: Numerical simulations

David C. Doughty[a,*], Steven C. Hill[a], Daniel W. Mackowski[b]

[a] US Army DEVCOM Army Research Laboratory, 2800 Powder Mill Rd., Adelphi, MD, USA
[b] Auburn University, Auburn, AL, USA

ARTICLE INFO

Article history:
Received 30 September 2020
Revised 19 December 2020
Accepted 19 December 2020
Available online 24 December 2020

Keywords:
SARS CoV-2
UV inactivation
Disinfection
Respiratory droplets
Shielding
Light scattering

ABSTRACT

UV radiation can inactivate viruses such as SARS-CoV-2. However, designing effective UV germicidal irradiation (UVGI) systems can be difficult because the effects of dried respiratory droplets and other fomites on UV light intensities are poorly understood. Numerical modeling of UV intensities inside virus-containing particles on surfaces can increase understanding of these possible reductions in UV intensity. We model UV intensities within spherical approximations of virions randomly positioned within spherical particles. The model virions and dried particles have sizes and optical properties to approximate SARS-CoV-2 and dried particles formed from respiratory droplets, respectively. In 1-, 5- and 9-μm diameter particles on a surface, illuminated by 260-nm UV light from a direction perpendicular to the surface, 0%, 10% and 18% (respectively) of simulated virions are exposed to intensities less than $1/100^{th}$ of intensities in individually exposed virions (i.e., they are partially shielded). Even for 302-nm light (simulating sunlight), where absorption is small, 0% and 11% of virions in 1- and 9-μm particles have exposures $1/100^{th}$ those of individually exposed virions. Shielding is small to negligible in sub-micron particles. Results show that shielding of virions in a particle can be reduced by illuminating a particle either from multiple widely separated incident directions, or by illuminating a particle rotating in air for a time sufficient to rotate through enough orientations. Because highly UV-reflective paints and surfaces can increase the angular ranges of illumination and the intensities within particles, they appear likely to be useful for reducing shielding of virions embedded within particles.

1. Introduction

Viruses such as influenza, measles, smallpox, SARS and some noroviruses can be transmitted via particles in the air. Improved methods to reduce the transmission of viruses are needed. Ultraviolet (UV) light can inactivate SARS-CoV-2 [58,67,68] and other viruses [31,32,62–64,71], and thereby help reduce transmission rates [1,46]. Solar UV radiation near the Earth's surface, primarily UVB at 280-315 nm, can inactivate SARS-CoV-2 [58,67] and other microbes [61]. UVC (200-280 nm) is common for germicidal applications [4,14,16,32,35,59,76].

Viruses may occur within droplets (liquid particles of any size) expelled from the upper or lower respiratory tract [37,47,49,66]. These droplets can range in size from submicron to greater than 10 μm in normal breathing and speaking [48] to 1000 μm in sneezing or coughing [3,7,10,17]. Such liquid particles tend to lose water rapidly under subsaturated conditions, with evaporation likely occurring in less than 0.8 s for liquid particles with diameters < 20 μm [48]. The resulting dried aerosol particles can range in size from submicron [39] to greater than 20 μm. At a relative humidity (RH) of less than 50% they can dry into somewhat spherical particles, at least for sizes smaller than 25 μm [75]. In using reported size distributions of droplets and particles of dried droplets it is useful to note the ranges of sizes measurable with the instrumentation, whether the humidity and time before measurement resulted in droplets or dried droplets, and whether the size distributions are given as particle number or particle mass.

The expelled droplets and dried particles may be inhaled or may land on surfaces and subsequently be transferred to nose, eyes, or mouth as part of the transmission of disease. Some viruses including SARS-CoV-2 can remain pathogenic in

* Correspondence author.
E-mail address: david.c.doughty2.civ@mail.mil (D.C. Doughty).

https://doi.org/10.1016/j.jqsrt.2020.107489

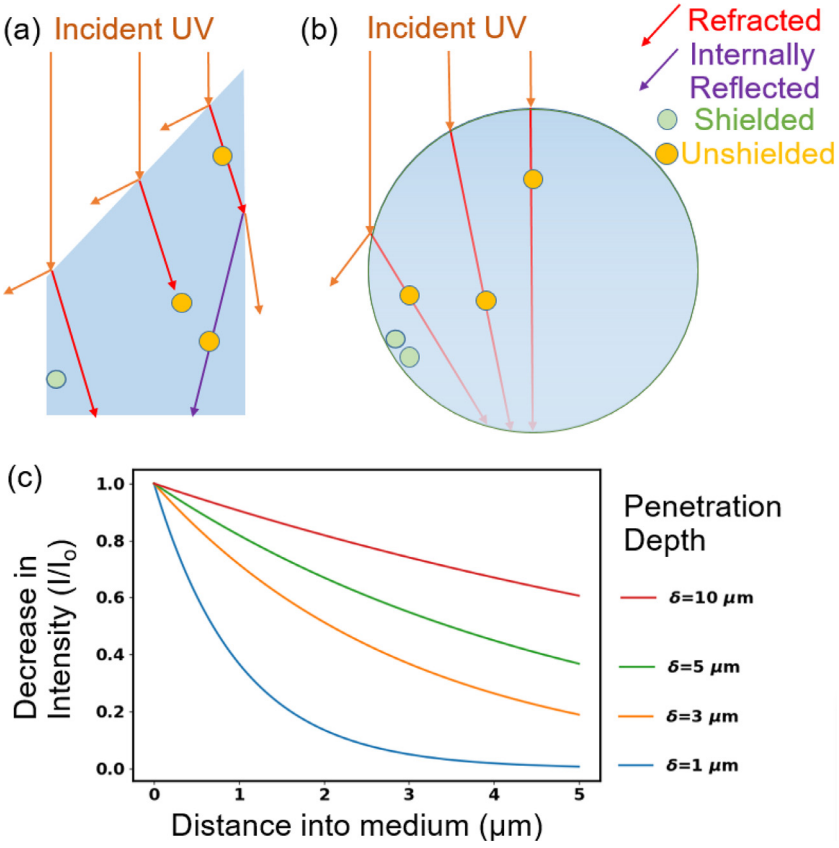

Fig. 1. Illustration of optical features related to shielding of microbes such as viruses in particles from UV light. The material surrounding the particles is air. (a) Refractive shielding in a non-spherical particle. (b) Refractive and absorptive shielding in a spherical particle. If the virions are 100 nm diameter and the drawing is to scale, the large sphere is approximately 2 μm diameter. (c) Decrease in intensity with distance into a medium as a function of penetration depth for δ similar to those used in this paper.

aerosol particles, either in air [45,67] or after landing on a surface [52,58,65,67,72]. Materials that were initially deposited from air may be reaerosolized (resuspended) [12,29,33,36,40,53,56,57]. Viruses and other microbes not initially deposited from air may be aerosolized (suspended in air) by toilet flushing, wind-gusts, waterdrop splashing, walking, or mechanical processes [15,26–28,38,70]. Some relevant surfaces for virus transmission include those in restaurants, restrooms, healthcare facilities, and personal protective equipment, including facemasks [12,77]. There are many uncertainties relating to the relative importance of different routes of transmission of viral diseases, including COVID-19. The relative importance of these modes depends upon the virus species, and can depend on factors such as the size distributions of virus-containing particles [8,66], the locations in infected persons where their viral loads are highest [78], airflows [7], humidity [45], and behaviors of the relevant persons. In the case of SARS-CoV-2, although many questions remain unanswered, there is considerable interest in using UV to inactivate virions on surfaces [58], and in air [5,14,20,50].

A microbe in a particle may be partially shielded from UV by other materials in the particle [18,30,51]. This shielding may result in microbes remaining infectious in particles even when the particles are exposed to sufficient UV light to inactivate the microbes when exposed individually. Such shielding can make germicidal UV more difficult in settings where microbes are in particles. An improved understanding of how virions in particles can be shielded from UV light could help in effectively using UV to deactivate SARS-CoV-2 and other microbes.

Optical phenomena affecting shielding of viruses from UV include the following (see Fig. 1): i) Absorption of UV causes the intensity to decrease as it travels into the particle and so reduces the intensity of UV reaching the virion. ii) Refraction of UV at a surface of a particle can direct light away from a virion; the importance of refraction depends upon the shape of the particle, the angle of the incident UV light with respect to the orientation of the particle, and on the optical properties of the particle and the material outside the particle. iii) Reflection at the outer surface of a particle can reduce the UV entering or exiting a particle; in inhomogeneous particles it can occur at surfaces separating regions within the particle. iv) Diffraction and scattering can increase UV intensities in regions which may otherwise be dark, in a ray optics approximation, because of refraction and absorption.

Models of the UV intensities in particles containing viruses can be useful in understanding UV inactivation and in improving UV decontamination systems. Valid models for the UV intensity within each virion can be combined with measured inactivation data to predict the numbers of virions likely to be inactivated within a particle. Validated models can predict results for large numbers of potential experiments that are impractical to perform in the laboratory or the field. Thus, such models can be essential tools for identification of decontamination techniques most appropriate for further testing.

In this paper we calculate the UV intensities in 100-nm-diameter spherical particles (approximating SARS-CoV-2 virions) located within an encompassing spherical particle simulating dried saliva or other airway fluid. The encompassing particles are on a surface or in air. The complex refractive index ($m = m_r + i\, m_i$) for the dried airway fluids and for SARS-CoV-2 virions are estimated using compositions of dried fluids and virions extracted from the literature and the optical properties of the various components similar to that in Hill et al. [23,24]. Both the simulated virions and

dried fluid particles are homogeneous in the simulations run here. The UV intensities within the virions within the dried droplets in this model problem are calculated using the Multi-Sphere T-Matrix (MSTM) method [41,43,44]. The MSTM provides an exact solution to the electromagnetic field equations (Maxwell's equations) for problems which include non-overlapping spheres within spheres, with or without a planar surface. The particles are illuminated by a UV plane wave at 260 nm or 302 nm. UV intensities within virions are calculated for three different encompassing particle sizes, plus the naked virion, as well as four different imaginary refractive indices for the encompassing fluid. Typically, illumination is from normally incident light, but in some cases illumination is from as many as five different directions or equally from all directions. These calculations can help in understanding the shielding of virions from UV, including: the wavelength-dependence of shielding; increases in shielding in larger sized particles; and reductions in shielding in particles illuminated from multiple angles.

2. Methods

2.1. Compositions of dried respiratory fluids and virions

Concentrations of components of saliva used here are selected to be representative of values reported by several sources [6,11,73,74]. The concentrations provided in Table 1.2 in [11] (a compilation of 20 sources) are used for inorganic electrolytes (Na^+, K^+, Mg^{2+}, Ca^{2+}, Cl^-, $PO_4{}^{3-}$, $HCO_3{}^-$, SCN^-, and F^-); non-UV-absorbing small molecules (glucose, lactate, lipids, urea, and ammonia); proteins and free amino acids; and the mucin glycoproteins. The concentration of protein used is 1.63 mg/ml. The combined concentration of mucins (MUC5B and MUC7) is 1.27 g/L, a concentration which includes both the amino acids and the carbohydrate of these glycoproteins. Typical mass fractions of airway mucin are 25% protein and 75% carbohydrate. Using these values, we calculated concentrations of carbohydrate in the mucins are 0.75 × 1.27 g/L = 0.95 g/L. Reported concentrations of DNA in saliva range from approximately 0.01 to 0.28 mg/ml [55]. The DNA concentration here is assumed here to be 0.12 mg/ml. Concentrations of RNA are assumed to be equal to those of DNA (0.12 mg/ml). We know of no reported measurements of non-viral RNA in saliva or nasal fluids. However, we assume that the DNA in these fluids arise from cells. Cells (human or bacterial) typically have several times as much RNA as DNA [23], and so the assumption of 0.12 mg/ml for RNA may be low. Hydrolysis of DNA or RNA by nucleases does not eliminate the UV absorption by the bases. The concentration of uric acid used is 0.024 mg/ml, in the range of values measured [2,19]. Peden et al. [54] demonstrate uric acid in nasal airway fluids.

Each virion is assumed to be 100 nm in diameter, where the outer 5 nm is a lipid bilayer. The virus genome, ssRNA (29,893 nucleotides, A=8954, T=9594, G=5863, U=5492) has a mass of 1.39×10^{-17} g, which is only 0.22% of the virion mass. The mass of the virion not in RNA or lipid is assumed to be protein, although we suspect other small UV-light-absorbing molecules such as uric acid or NAD may be enclosed within the virion.

2.2. Optical properties of the dried respiratory fluids and virions

The primary optical property needed for modeling the UV in particles is the complex refractive index, $m = m_r + im_i$. The imaginary part of m is defined as $m_i = \lambda/4\pi\delta$, where λ is the free-space wavelength, and δ is the penetration depth, a key parameter useful in understanding shielding by absorption. If I(z) is the intensity (I) of a UV planewave at distance z in a homogeneous medium, the fraction of light remaining at z is $I(z)/I_0 = e^{-z/\delta}$, where the intensity at z=0 is I_0, and δ is the distance at which the UV has decreased to 1/e (= 0.368) of I_0. Also, $m_i = \lambda c\varepsilon/4\pi$, where c is the concentration of the absorbing material and ε is the molar absorption coefficient [25], also termed absorptivity [22–24], molar absorptivity, molar extinction coefficient or molar attenuation coefficient. The molar absorption coefficients of biological materials at the wavelengths used were estimated from the literature as described previously [22–24].

The density of the dried solids is estimated as a weighted average of the densities of materials in the droplet. Using the concentrations of materials within the droplet, and the density of the dried particle, the concentrations of the relevant materials in the dried droplet are calculated. The contribution of the j^{th} material to the total m_i of the dry particle, i.e., $m_{i,j}$ is then is calculated using the concentration (g/g) and the extinction coefficient for the material as described previously [23,24]. The total m_i is the sum of the $m_{i,j}$. The main UV-light-absorbing materials in the 260 to 302 nm range in airway fluids are tryptophan and tyrosine (primarily in proteins), nucleic acids, and uric acid [19]. At longer wavelengths the absorption by proteins, nucleic acids and uric acid tend to be so low that the penetration depths δ are many times larger than the diameter of most dried particles.

In calculating the m_i for virions, the average amino acid composition is taken as the average of all the amino acids specified by the genome. The different proteins are not weighted by their copy number or mass fraction mainly because we do not have values for these mass fractions. For the calculations of the UV absorbed by virions, each virion is assumed to be homogeneous. The code to calculate the m_r and m_i used here is similar to that described previously [22–24].

2.3. Morphology of the dried particles from droplets containing virions

Droplets of airway fluids are assumed to be generated by sneezing or coughing. Their properties are assumed to be consistent with those of saliva or nasal fluids. The expelled droplets are assumed to dry into spherical particles; the dried particles of simulated saliva studied by Vejerano and Marr [75] appeared to be somewhat spherical, at least for particles smaller than 25 μm. The dissolved solids in saliva are assumed to be 6 mg/cm^3 (0.006×10^{-12} g/μm^3), in the range of reported values [11,75]. We assume a density for the dry particle of 1.5 g/cm^3 (1.5×10^{-12} g/μm^3). For these values, droplets with diameters of 6.3, 31.5, and 56.7 μm, dry to particles with diameters of 1-, 5- and 9-μm respectively, the sizes studied here.

Virions comprise at most a very small fraction of the mass of the solids in airway fluids. The concentrations of SARS-CoV-2 virions measured in COVID-19 patients and healthcare workers [78] ranged from 4×10^4 to 4×10^{10} copies/mL in saliva and up to 5×10^9 copies/mL in nasal fluids. The mass of a 100 nm diameter virion having an assumed density of 1.2 g/mL is 6×10^{-13} mg. The mass of 4×10^{10} of these virions (highest number measured in 1 mL by Wyllie et al. [78]) is 0.024 mg, i.e., 1/240th the mass of the other solids in the typical saliva assumed here. For the properties described in the previous paragraph, the maximum average numbers of virions per dried 9-μm particle is 3680 and in a dried 5-μm particle is 630. For almost all the other cases reported by Wyllie et al. [78], the concentration of virions is orders of magnitude smaller, and the majority of sneezed or coughed droplets resulting in dried particles in the 1- to 9-μm range would have no virions. The location of virions within dried droplets of airway fluids has not been measured, so far as we know. We assume the virions are randomly distributed throughout the dried respiratory droplet.

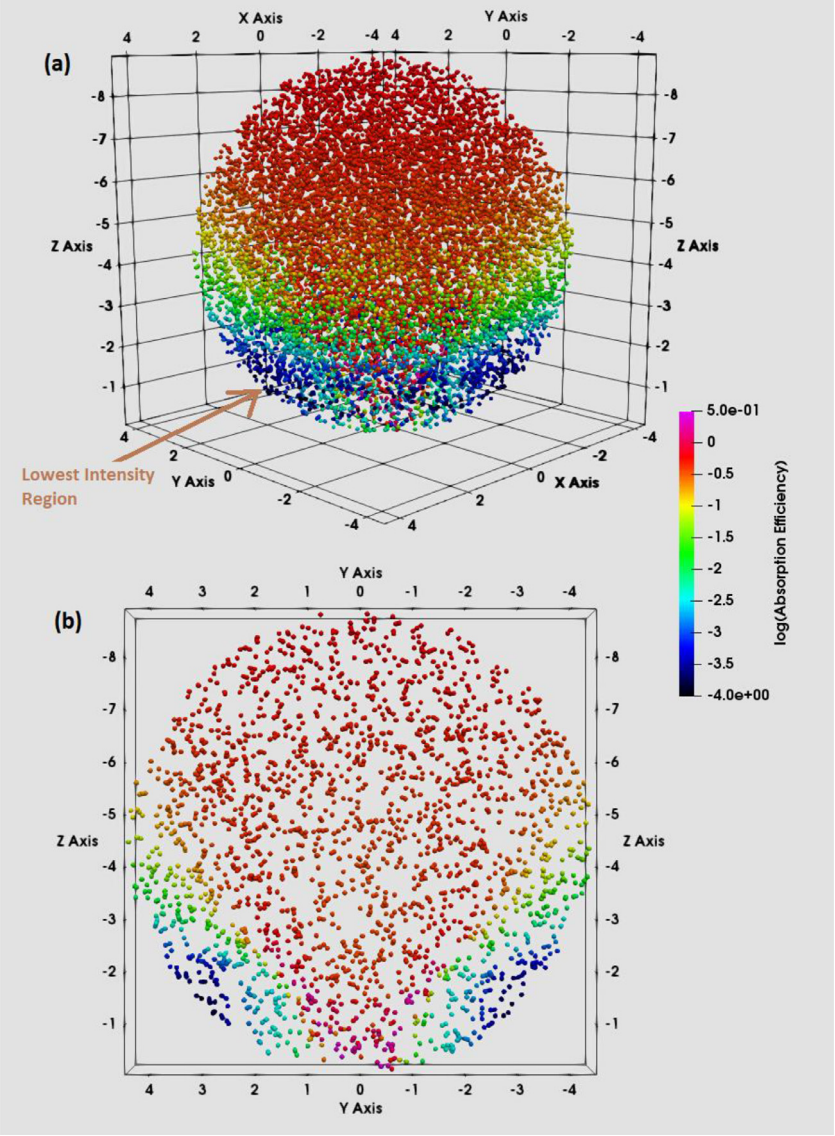

Fig. 2. The spatial distribution of virions in 3D within a 9-μm diameter sphere approximating a spherical particle of dried airway fluids. The color of each virion indicates the R_i, the relative UV intensity within that virion, and is proportional to the rate of absorption of UV energy by that virion. The incident UV light propagates downward from the top of the page, in the z direction. The surface begins at z=0. For all z<0 and not inside the dried droplet the material is air. Results were calculated using the MSTM. The outer edge of the larger particle is not shown, but is just outside the outermost virion locations. The R_i were calculated using 120 sets of 100 virions each. B: A slice through the center of the sphere including all virions with $-0.5 < x_{center} < 0.5$ μm.

2.4. MSTM calculations of UV intensities in virions inside a particle on a surface or in air

In this paper the UV intensities in the spherical particles were calculated by solving the electromagnetic field equations (Maxwell's equations) for a number of homogeneous spheres, separate or included within other spheres, and with the potential of being in contact with a flat surface, all illuminated by one or more plane waves [41,43,44]. In the MSTM as used here, a plane wave with irradiance I_o (or set of n plane waves with irradiance I_o/n for each wave) illuminates either a naked virion or a spherical particle which contains a number of virions. The net rate of energy absorption by the i^{th} virion is $I_o \pi a_i^2 Q_{abs,i}$, where a_i is the radius and $Q_{abs,i}$ is the absorption efficiency, each for the i^{th} virion. The focus in this paper is on the absorption of UV energy by virions in the large particle relative to virions resting on (or very near, i.e., 10 nm) the surface. A main quantity illustrated here is the relative rate of absorption of UV energy of the i^{th} virion, $R_i = Q_{abs,i} / Q_{abs,single}$ where $Q_{abs,single}$ is the absorption efficiency of an individual virion resting on the same surface. Because the diameters and m for all virions in a given simulation are identical, R_i is the relative UV intensity within the i^{th} virion. The illumination used in the calculations is unpolarized because sunlight and UV lamps are unpolarized. When multiple illumination angles of incidence are used, each R_i is calculated for each virion for each angle of incidence with respect to a naked virion on the same surface illuminated with normally incident light. For each virion, R_i from the different angles of incidence are averaged.

3. Results: UV intensities in virions in particles of dried airway fluids on a surface

3.1. UV intensities in virions in particles illustrated in 3D

Fig. 2 illustrates a 3D plot of 12,000 virions (calculated as 120 sets of 100 virions each) randomly positioned within a 9-μm sphere simulating a dried saliva particle. The 12,000 virions are used to illustrate the position-dependent variations in UV energy

Table 1
For dried droplets of respiratory fluids, the approximated concentrations (mass%) of the main UV absorbing materials and contributions to the imaginary part of the refractive index (m_i) (total and percentage). The wavelengths used are in the top row. In the bottom three rows are the complex refractive index and the penetration (skin) depth.

		260 nm		302 nm	
Material	%mass from material	m_i from material	$\%m_i$ from material	m_i from material	$\%m_i$ from material
Tryptophan	0.35666	0.000412	5.6577	0.000026	1.0744
Tyrosine	0.74305	0.000157	2.1543	0.000003	0.1261
Phenylalanine	0.53499	0.000062	0.8507	0.000000	0.0000
Protein	29.72181	0.000631	8.6627	0.000029	1.2005
DNA	2.07869	0.002647	36.3605	0.000000	0.0000
RNA	2.07869	0.003309	45.4506	0.000000	0.0000
NADH	0.00066	0.000001	0.0123	0.000000	0.0061
FMN+riboflavin	0.00046	0.000002	0.0237	0.000000	0.0046
Uric acid	0.67557	0.000691	9.4903	0.002378	98.7887
Other	65.44411	0.000000	0.0000	0.000000	0.0000
Total	100	0.00728	100	0.002407	100
Re(Ref. Indx)		1.601		1.586	
Im(Ref. Indx)		0.007280		0.002407	
Skin depth (μm)		2.842		9.984	

Table 2
For virions, the approximated concentrations (mass%) of the main UV-absorbing materials and contributions to the imaginary part of the refractive index (total and percentage). The wavelengths are in the top row. In the bottom three rows are the complex refractive index and penetration (skin) depth.

		260 nm		302 nm	
Material	% mass from material	m_i from material	$\%m_i$ from material	m_i from material	$\%m_i$ from material
Tryptophan	1.08750	0.001256	59.1656	0.000079	85.2596
Tyrosine	1.59500	0.000337	15.8599	0.000007	7.0469
Phenylalanine	1.30500	0.000151	7.1173	0.000000	0.0000
Cystine	0.36250	0.000029	1.3592	0.000002	2.4157
Protein	72.50000	0.001772	83.5020	0.000088	94.7221
RNA	0.22000	0.000350	16.4980	0.000005	5.2779
Lipids	27.20000	0.000000	0.0000	0.000000	0.0000
Other	0.07999	0.000000	0.0000	0.000000	0.0000
Total	99.99999	0.002123	100	0.000092	100
Re(Ref. Indx)		1.59		1.575	
Im(Ref. Indx)		0.002123		0.000092	
Skin depth (μm) δ		9.747		259.852	

absorbed by the virions, not because a 9-μm particle is likely to carry such a large number of virions. A large number of virions are needed to represent the distribution well. The m_r and m_i used for the calculations are as shown in Table 1 for the dried saliva, and in Table 2 for the virions. The particle is present on a surface with m=1.4+i 0.0001. The particle is illuminated with 260-nm light which propagates downward (from the top of the figure) in a direction normal (perpendicular) to the surface. The illumination is unpolarized for this normal-incidence case, and so the intensity distribution would be independent of the angle around the sphere axis aligned with the direction of wave propagation if the sphere were perfectly homogeneous. The virions are color coded according to R_i, the relative rate of absorption of UV energy by the i^{th} virion relative to an isolated virion on the same surface (see Section 2.4). Also, the lowest intensity regions, indicated by colors from turquoise to black, have UV absorption efficiencies that are over two orders of magnitude smaller than the UV absorption of an individual virion on a surface. In these figures, the shielded regions result from a combination of absorptive and refractive shielding.

The highest intensities in Fig. 2 are at the top of the dried droplet (where the incident beam first encounters the particle), along a cone formed as the light is focused by the first illuminated surface of the encompassing sphere, and along an axis of the droplet in the direction of propagation of the wave (normal to the planar surface) which passes through the center of the sphere. The intensity of the cone increases as its radius decreases as it descends through the droplet and partially reflects internally from the droplet surface as visualized using geometrical optics [9]. The most shielding from UV occurs in the outer edge of the particle on the side away from the incident light. Virions at the center of the particle are negligibly shielded by refraction from UV.

The sensitivity of the distributions of the R_i to the numbers of virions in a dried particle was examined by calculating the R_i for particles with 4000, 3000, 2000, 1000, 500, 250, 100, 50, 25, and 10 virions. Effects of changes in virion numbers on the distribution of R_i calculated were below 0.5% until over 100 virions were used in a 9-μm dried droplet (Fig. S1) and 25 virions in a 5 μm dried droplet (Fig. S2).

3.2. Distributions of virion numbers vs UV intensity for particle diameters of 0.1, 1, 5 and 9 μm

With either 260- or 302-nm illumination the extent of shielding decreases as particle size decreases (in moving in Fig. 3 from the top to the bottom panel in either column, or in moving from 3a to 3d or 3e to 3h in Table 1). For example, at 260 nm, in the 9-μm particle, 29.6% of virions have $R_i < 0.1$ and 6.4% have $R_i < 0.001$; in the 5-μm particle, 24.2% of virions have $R_i < 0.1$ and 10% have $R_i < 0.01$, but none have $R_i < 0.001$; in the 1-μm particle over 31% of the virions have $R_i > 1.0$, and 0.2% have $R_i < 0.1$. In the limiting case of the 0.1 μm naked virion there is no shielding (Table 3).

In the panels on the right of Fig. 3(d–g) with 302-nm illumination, the virions are less shielded from UV than at 260 nm, especially for the 5- and even more for the 9-μm particles. The differences between the extent of shielding at 260 nm vs 302 nm are primarily because the penetration depth is several times larger in the case of 302 nm illumination. The lower m_r at 302 nm also

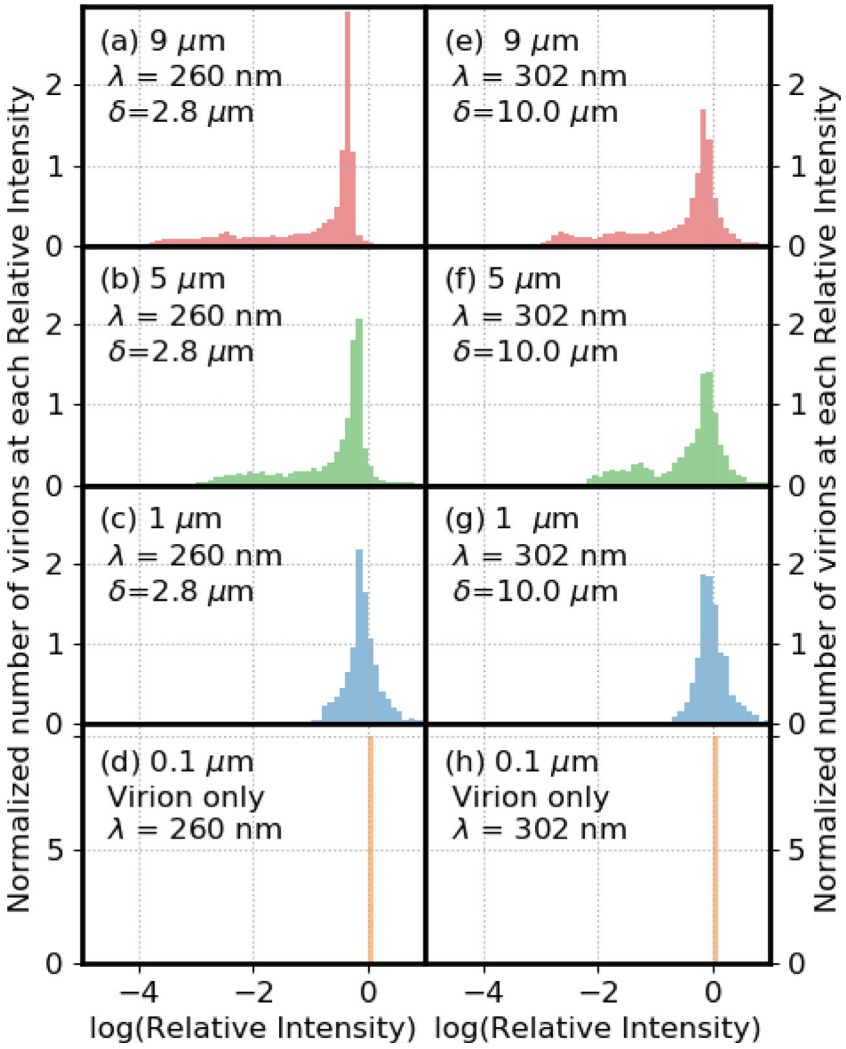

Fig. 3. Numbers of virions in bins with the log(relative UV intensity) shown. Particle diameters are 9 μm in (a) and (e), 5 μm in (b) and (f) and 1 μm in (c) and (g). Particles are on a surface with m=1.4 + i 0.0001. The wavelength is 260 nm for the panels on the left and 302 nm for the panels on the right. Penetration depths (δ) are stated for each panel. The area under each distribution is normalized to 1.

contributes to the reduction in shielding, but contributes less than does the decrease in m_i.

3.3. Distributions of virion numbers vs UV intensity for different penetration depths

Fig. 4 illustrates distributions of numbers of virions in different relative-UV-intensity bins vs relative-UV-intensity (log scale) for 9-μm particles shown in order of increasing m_i. In all cases the particles are on a surface with m = 1.4+i 0.0001. In moving from top to bottom, the penetration depths decrease from 59.9 to 9.98 to 2.84 to 1.42 μm. Of these δ, the center two are as in Table 1 for 302 and 260 nm respectively. The δ in the top panel of Fig. 3 is six times the δ given in Table 1 for 302 nm. The bottom panel has a δ of ½ the δ estimated for 260 nm (in Table 1).

In moving from panel a) to d) the center value of log(R_i) of the bin with the highest number of virions decreases as follows: -0.05, -0.15, -0.35, -0.85. In the case with the lowest m_i 58.7% of the virions have R_i greater than 0.5, and none have $R_i < 0.001$. As the m_i increases, R_i decreases, and for the most absorbing case, 11.8% of virions have $R_i < 0.001$ and 1.9% have $R_i < 0.0001$ (Table 3). The 9-μm particles are illustrated because the shielding is largest in these particles, as seen in Fig. 3.

3.4. Distributions of virion numbers vs UV intensity for illumination from different angles from the zenith

Fig. 5 illustrates distributions of numbers of virions in different relative-UV-intensity bins vs relative-UV-intensity (log scale) for three incident angles (β) relative to the vertical, also termed the zenith angle. In Fig. 5a–c, $\beta = 0°$, 40° and 80° respectively. For these angles, the percentage of virions with $R_i < 0.1$, $R_i < 0.01$, and $R_i < 0.001$ is approximately 30%, 15%, and 5% respectively (Table 3). However, although there are no virions with R_i below 0.0001 at an incident angle of zero degrees, at 80°, approximately 1% of the virions had relative intensities below 0.0001. Also, when $\beta = 80°$ there are a higher number of virions with $R_i > 0.8$ (Table 3). The 9-μm particles are illustrated for the different angle analysis because the shielding is largest in these particles, as in Fig. 3.

3.5. Illumination from multiple angles sequentially or simultaneously

Fig. 6 illustrates normalized distributions of numbers of virions in R_i bins for virions in a 9-μm particle on a surface illuminated by one- to five-planewaves. The illumination could be simultaneous or sequential: the resulting total UV intensities within virions are identical because the UV light source is not coherent. In Fig. 6a the illumination is from above the sphere (β =0°). In Fig. 6b the angles

Table 3
Percentage of virions below relative intensity of 1, 0.8, 0.5, 0.1, 0.01, 0.001, 0.0001. Wavelength (λ), m_i, angle, orientation, and number of particles are shown. The wavelength is in units of nm, diameter is in units of microns. For orientation, "F" means Fixed, "All" means averaged over all orientations, "S" means on a surface, and "A" means in air. The percentages are shown in green in the table.

Fig	λ nm	d μm	N	m_i	angle degrees	%R_i < 1.0	%R_i< 0.8	%R_i< 0.5	%R_i < 0.1	%R_i< 0.01	%R_i< 0.001	%R_i < 0.0001
3a	260	9	12000	0.00728	β=0,α=0	99.0	98.4	85.3	29.6	17.5	6.4	0
3b	260	5	3000	0.00728	β=0,α=0	94.4	90.1	51.1	24.2	10.0	0	0
3c	260	1	500	0.00728	β=0,α=0	68.2	52.2	20	0.2	0	0	0
3d	260	0.1	1	0.00728	β=0,α=0	0	0	0	0	0	0	0
3e	302	9	12000	0.00728	β=0,α=0	84.2	71.6	44.9	25.8	10.7	0.06	0
3f	302	5	3000	0.00728	β=0,α=0	76.1	62.6	41.2	21.1	1.9	0	0
3g	302	1	500	0.00728	β=0,α=0	55.8	38.4	10.6	0	0	0	0
3h	260	0.1	1	0.00728	β=0,α=0	0	0	0	0	0	0	0
4a	302	9	12000	0.0004	β=0,α=0	71.8	59.5	41.3	22.8	3.5	0	0
4b	302	9	12000	0.00241	β=0,α=0	84.2	71.6	44.9	25.8	10.7	0.06	0
4c	260	9	12000	0.00728	β=0,α=0	99.0	98.4	85.3	29.6	17.5	6.4	0
4d	260	9	12000	0.01456	β=0,α=0	100.	100.	96.8	41.1	19.7	11.8	1.9
5a	260	9	12000	0.00728	β=0,α=0	99.0	98.4	85.3	29.6	17.5	6.4	0
5b	260	9	12000	0.00728	β= 40, α = 0	98.9	98.5	83.0	28.7	14.7	4.7	0.3
5c	260	9	12000	0.00728	β= 80, α = 0	88.1	78.3	63.9	30.1	15.8	6.1	1.0
6a	260	9	12000	0.00728	β=0,α=0	99.0	98.4	85.3	29.6	17.5	6.4	0
6b	260	9	12000	0.00728	β= 0,40, α = 0	99.3	98.7	86.3	24.5	9.1	0.9	0
6c	260	9	12000	0.00728	β= 0,80, α = 0	98.7	95.6	70.7	18.7	6.8	1.4	0
6d	260	9	12000	0.00728	β= 80, α = 0,180	95.8	89.2	64.1	12.4	0.4	0.1	0
6e	260	9	12000	0.00728	β= 80, α=0,90,180,270	98.3	92.0	64.4	8.5	0.3	0.1	0
6f	260	9	12000	0.00728	β=0,α=0 + β= 80, α= 0,180	98.7	95.4	71.7	10.3	0.2	0	0
6g	260	9	12000	0.00728	β=0,α=0+ β= 80, α=0,90,180,270	99.6	96.1	70.0	6.9	0.03	0	0
7a	260	5	3000	0.00728	All	100	70.7	56.2	0	0	0	0
7a	260	5	3000	0.00728	β=0,α=0 A	91.9	84.3	45.8	22.8	8.6	0	0
7a	260	5	3000	0.00728	β=0,α=0 S	94.4	90.1	51.1	24.2	10.0	0	0
7b	260	9	4000	0.00728	All	100	100	90.9	0	0	0	0
7b	260	9	12000	0.00728	β=0,α=0 A	98.6	98.1	72.4	28.7	16.6	6.7	0.03
7b	260	9	12000	0.00728	β=0,α=0 S	99.0	98.4	85.3	29.6	17.5	6.4	0

(β, α) are (0°, 0°) and (40°, 0°) (the azimuthal angle is α). In Fig. 6c the two incident waves are defined by angles (0°, 0°) and (80°, 0°). In Fig. 6d the two incident waves are given by (80°, 0°) and (80°, 180°). In each of these four cases ((a) to (d)), between 29.6% and 12.4% of virions have R_i below 0.1 (Table 3), with the percentage with R_i below 0.1 decreasing as the angle between the two beams increases in Fig. 6b-d.

In each of the last three panels, three or more incident UV waves are used and the percentage of particles with $R_i > 0.1$ increases as additional beams are added. In Fig. 6e four UV waves are incident, from angles (80°, 0°), (80°, 90°), (80°, 180°) and (80°, 270°); 8.5% of virions have $R_i < 0.1$; and the minimum R_i is 0.0002. In Fig. 6f, three incident waves are used: two planewaves propagating primarily toward each other (at angles (80°, 0°) and (80°, 180°)), and the third wave traveling perpendicular to the surface. In this case, 10.3% of particles have $R_i < 0.1$, and the minimum R_i is 0.004. In Fig. 6g the particle is illuminated by five planewaves: one is normally incident; the other four have β=80° and azimuthal an-

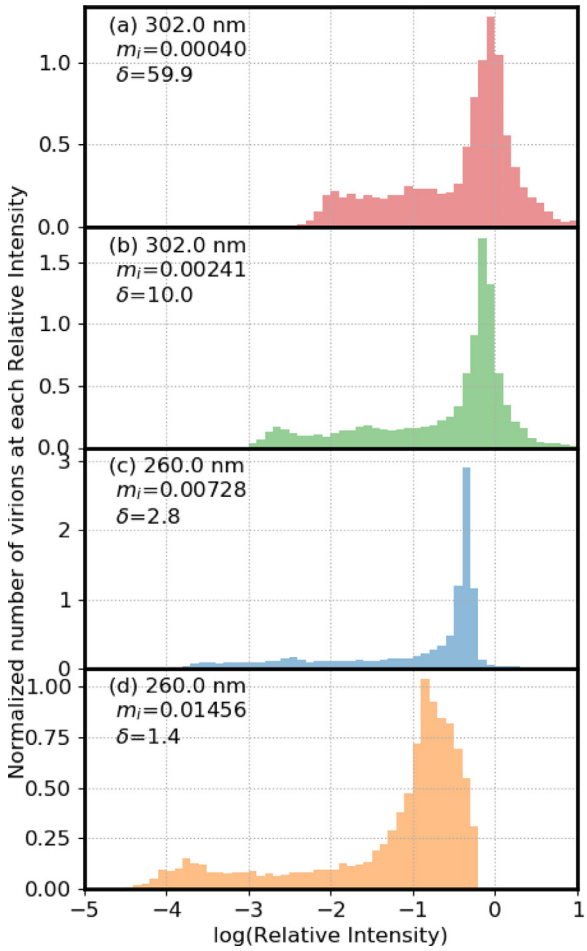

Fig. 4. Numbers of virions in bins with the log(relative UV intensity) shown. The particles are 9-μm diameter and resting on a surface with m= 1.4 +i 0.0001. In all cases the number of virions (N) is 12000. (a) m_i = 0.000401, δ=59.9 μm; (b) m_i = 0.002407, δ=9.984 μm; (c) m_i = 0.007280, δ=2.842 μm; (d) m_i = 0.01456, δ=1.421 μm. The area under the distributions is normalized to 1.

gles = 0°, 90°, 180° and 270°. That is, the angles of the five waves are: (0°, 0°), (80°, 0°), (80°, 90°), (80°, 180°), and (80°, 270°). In this case, 6.9% of the particles have R_i < 0.1, and the minimum R_i is approximately 0.009.

For an objective of illuminating every virion in such particles with at least some desired UV intensity, these results suggest that illuminating with multiple widely-separated waves as illustrated in Fig. 6d and e, and especially in Fig. 6f and g, could provide a way to achieve that goal with lower total UV energy than needed for illumination with only one or two beams separated by ≤ 80°.

3.6. Particles in air illuminated from all directions

Fig. 7 illustrates normalized distributions of numbers of virions in R_i bins (log scale). The solid-color bars show the distributions for virions in particles averaged over all orientations with respect to an incident UV planewave (equivalent to illuminating particles with equal-intensity UV-light from all directions). The orientation averaged intensities are calculated as described by Mackowski and Mishchenko [42,43]. Also shown in Fig. 7 are the UV distributions for the fixed-orientation cases (shown with thin lines), on a surface and in air.

In the particles averaged over all orientations, no 5- or 9-μm particles have R_i < 0.1. In contrast, the fixed-orientation 5-μm particles have 8.6 and 10% of virions with R_i < 0.01 (in air and on the surface, respectively). The 9-μm particles have 16.6 and 17.5% of virions with R_i < 0.01 (in air and on surface, respectively) and have 6.7 and 6.4% of virions with R_i < 0.001 (see Table 3). That is, for an airborne UV-illuminated 9-μm particle with the properties used here, which rotates through enough angles such that it is approximately illuminated uniformly by UV light from all directions, the best shielded virions are still exposed to a UV intensity approximately $1/7^{th}$ of that of a clean individual virion. If that same 9-μm particle were held on a surface, or illuminated for such a short time that it could change orientation very little, then approximately 17% of the virions are shielded so that their exposure to UV is less than $1/100^{th}$ of that of a clean individual virion.

Airflows are turbulent in most situations where UV light is used to inactivate viruses in air. Particle orientation with respect to a UV light source can vary by "spinning" (i.e., rotating about a particle axis), or by "tumbling" (i.e., rotation of the axis of the particle), or by following the airflow. Particles undergo Brownian translational and rotational diffusion [13] even in a small closed container. The extent to which the UV in a particle is equivalent to the orientation-averaged results depends upon the airflows (including turbulence), Brownian rotational diffusion, particle size, time of exposure, and the position(s) and spatial extent(s) of sources of UV light. For a sufficiently short illumination time and slow enough particle rotation, particle rotation during illumination is negligible and the particle is essentially illuminated from one angle, as if it were "fixed in air".

4. Discussion

4.1. Virions in particles can be partially shielded from UV light

4.1.1. Particles on a surface: UV Illumination from one direction

a) Shielding increases with particle diameter as illustrated in Fig. 3 for 0.1, 1-, 5-, and 9-μm diameter particles. This increase occurs both with 260 and 302 nm light. Shielding of virions within the 1-μm particles is small compared with that in larger particles: only 0.2% of the 1-μm particles at 260 nm have R_i < 0.1. Absorptive shielding tends to become more important with increasing size because, on average, the UV energy must travel further through the particle to reach the virions, and so the light is more strongly attenuated prior to reaching a given virion.

b) Shielding of virions can be very significant even in weakly absorbing particles. Even when the penetration depth is 6.7 times greater than the particle diameter (Fig. 4a), 3.5% of the particles have R_i < 0.01 and 22.8% have R_i < 0.1. At such large ratios of δ/d the shielding is largely refractive. As the penetration depth of the dried respiratory fluids decreases from 59.9 μm to 10.0, 2.8, and 1.4 μm, the percent of R_i < 0.001 increases from 0.0 to 0.06, 6.4 and 11.8%, respectively.

c) Shielding of virions from UV light occurs with both the germicidal (260 nm) and solar (302 nm) wavelengths studied. Such shielding tends to be more significant at 260 nm where biological materials are more absorbing.

d) For virions in a sphere held in a fixed position, either in air or on a surface with m_r = 1.4, the differences in the UV in the virions in these two cases is relatively small. This finding holds for both the 5- and 9-μm diameter particles illustrated.

4.1.2. UV Illumination from multiple directions can reduce shielding from UV

UV intensities within refractively shielded regions can be increased by illuminating the particles from widely separated angles (Fig. 6d–g), in cases where such illumination is possible. Wide-angle illumination can be achieved to varying degrees by using

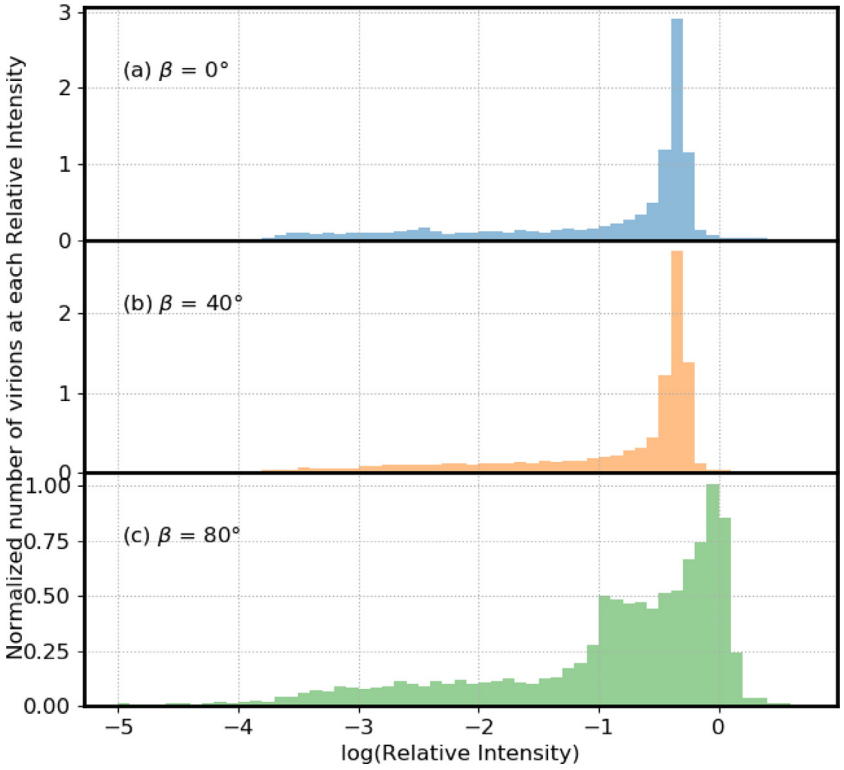

Fig. 5. Numbers of virions in bins with the log(relative UV intensity) shown. Particle diameters are 9 μm. The wavelength of the incident UV light is 260 nm. Particles are on a surface with m=1.4 + i 0.0001. In (a) the UV light is incident perpendicular to the plane (blue). In (b) the UV light is incident from 40 degree from the normal (yellow). In (c) the incident UV is 80 degree from the normal (green). The area under each distribution is normalized to 1.

multiple UV light sources, and/or using movable or robotically controlled sources. Equal magnitude waves propagating in opposite directions have been used previously to increase the light intensities in the regions of lowest intensity in a sphere [21]

4.1.3. Particles in air may rotate to be UV illuminated from many directions

Shielding of virions in particles illuminated from all directions or that rotate (spin and/or tumble) through all orientations is orders of magnitude smaller than in singly illuminated, fixed-position particles (Fig. 7). Absorptive shielding can still be significant in such cases. Whether or not an airborne particle of a certain size rotates through enough angles to have a only small amount of refractive shielding and a smaller effect of absorptive shielding depends on the particle size and shape, the illumination times, positions of the UV lights, and airflows (turbulent, laminar, circuitous or straight).

4.2. Variations and uncertainties in particles and their potential effects on the findings

Variations in compositions and morphologies of virus-containing particles exist even for dried droplets of sneezed or coughed respiratory droplets.

4.2.1. Variations and uncertainties in composition and complex refractive index of airway fluids

Estimating the m_i of saliva or other respiratory fluids from reported compositions of such fluids is not trivial. No one source provides all the relevant concentrations. It is not sufficient to know only the concentrations of the UV-absorbing materials in saliva, which would be adequate for estimating the m_i for the aqueous solution. The material for which the m_i is needed is the dried droplet. In the dried droplet, the concentrations of the UV-absorbing material (and thus the m_i) depend upon the concentrations of all the materials in the dried droplet. The best source we know for concentrations (with error bars) of the materials in saliva is Edgar et al., [11], especially Table 1.2, including the papers cited for the values. However, that table does not include uric acid or nucleic acids (including DNA, RNA, or other several other UV absorbing materials such as NADH, nucleosides, or vitamins). In our estimates of concentrations and m_i in Table 1, for dried droplets of respiratory fluids, uric acid is responsible for 98% of the m_i for saliva at 302 nm and 9.4% of the m_i at 260 nm. DNA, RNA and any other nucleic acids are responsible for 82% of the m_i at 260 nm. Because the DNA concentrations in saliva vary over a wide range (from 0.01 to 0.28 mg/ml, as measured by Poehls et al. [55]), and there is little if any reason to think RNA and ribonucleoside concentrations vary less widely, the m_i of dried particles of saliva appear likely to vary over large ranges. DNA and RNA in saliva occur primarily from breakdown of immune cells and bacteria. Cells tend to have several times more RNA than DNA, but once the cell is broken the RNA is more rapidly degraded. Thus, there is considerable uncertainty in the concentrations of chemical species in dried airway droplets.

The aromatic amino acids that are responsible for 8.8% of m_i at 260 nm (Table 1) occur primarily in the protein fraction of mucins, and to a lesser extent in albumin, immunoglobulins, and enzymes such amylase and lysozyme. Different mucins and enzymes predominate in different parts of the airways. The different salivary glands secrete different mucins and enzymes, or different concentrations of these. Even for a single person the concentrations of different inorganic ions, different mucins and other proteins, uric acid, DNA, etc., may depend upon hydration, exercise, odors, time of day and time since last drink or meal. The concentrations of various chemical species in airway fluids vary from person to person, as does the bacterial microbiome [2,11,19].

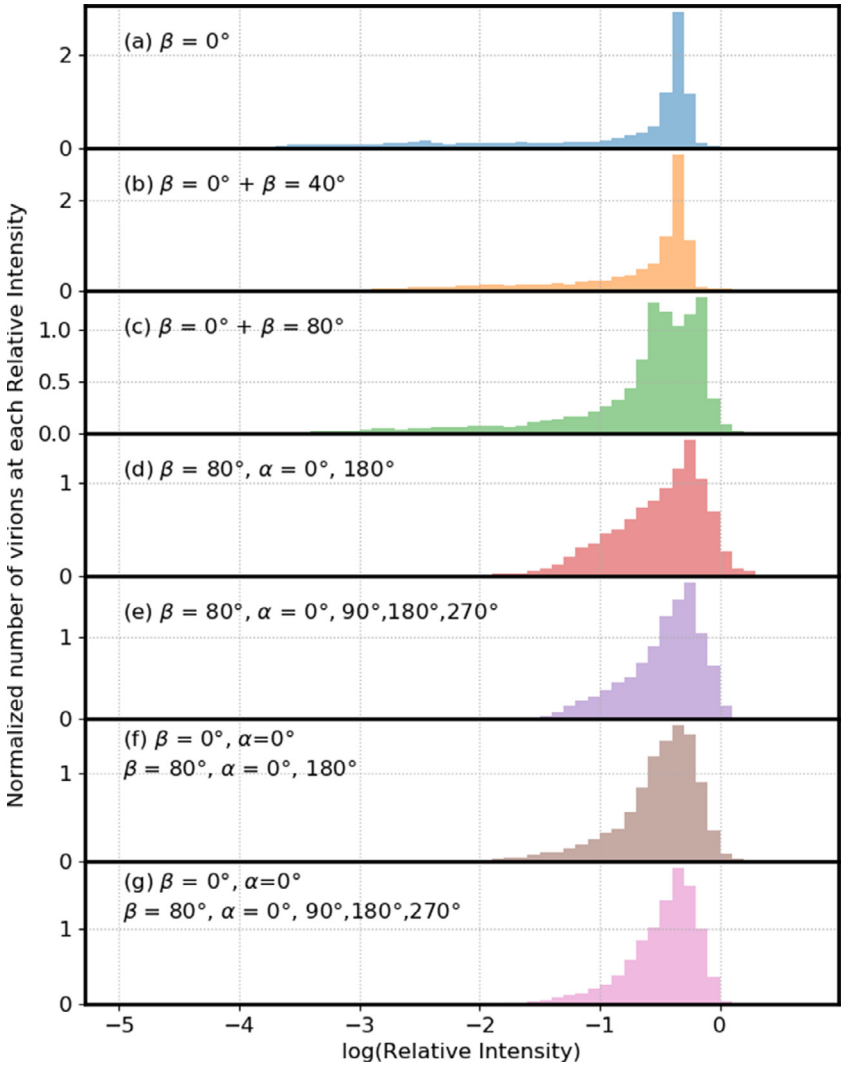

Fig. 6. Numbers of virions in bins with the log(relative UV intensity) shown. Particle diameters are 9 μm. The wavelength of the incident UV light is 260 nm. Particles are on a surface with m=1.4 + i 0.0001. In (a) the UV light is incident perpendicular to the surface (blue). In (b) one UV wave is normal to the surface and the other is 40° from the normal. In (c) one UV wave is normal to the surface and the other is 80° from the normal. In (d) both waves are incident 80° from the normal to the surface but the azimuthal angle is 0° in one and 180° in the other. In (e) four waves, all incident at 80° from the normal, are used. They differ in having azimuthal angles of 0°, 90°, 180° and 270°. In (f), three incident UV waves are used, the two waves as in (d) but also with the normal-incidence wave of (a). In (g), five incident UV waves are used: the four waves as in (g) but also with the normal-incidence wave of (a). Each incident UV plane wave has the same intensity. To compute the intensities within virions the intensity for each angle of incidence is averaged. The area under each distribution is normalized to 1.

4.2.2. Humidity-dependent variations in water content of dried particles

The particles here were assumed to be very dry, as in very low-humidity, desert environments. Vejerano and Marr [75] showed that as droplets of simulated saliva were exposed to lower RH, they lost water and decreased in size. For the particles modeled here, at least for water contents above some low level, higher RH would result in higher water contents of the dried particles. Such increased water contents and particle volumes would result in lower densities, lower concentrations of light-absorbing materials (g/g in the dried particle), and larger penetration depths. However, a variety of proteins at their lowest water contents (less than about 6 to 10%) increase in volume as the water is removed [69]. So, at the lower water fractions, 0 to possibly 10%, it is not clear whether the density would continue to increase the water decreases. Sirotkin et al. [69], wrote about hydrating very dry proteins: "The hydration of charged and polar groups causes a decrease in volume." Saliva and other airway fluids are complex mixtures which contain multiple inorganic and organic ions, mucins, nucleic acids, etc. These solutes have many charged and polar groups. Thus, it is possible that at very low water contents, the density could decrease as water content decreases.

4.2.3. Approach to mitigating the effects of uncertainties in m_i on calculated results

Variations and uncertainties in the densities and compositions of the dried particles may be the largest sources of differences between the calculations illustrated here and any specific particle of dried respiratory fluids. To account for such variability the model results were calculated for additional m_i which increased the range of penetration depths used from 2.8 to 10 μm (Fig. 3), to 1.4 to 59.9 μm (Fig. 4). While the actual composition of a real dried saliva drop might be different than the compositions used here, the results should be general enough to apply to some degree. Even though the variations in concentrations of materials measured in saliva and other airway fluids are not small, the absorptive and refractive shielding illustrated here are general phenomena useful for understanding how virions may be protected from UV radiation.

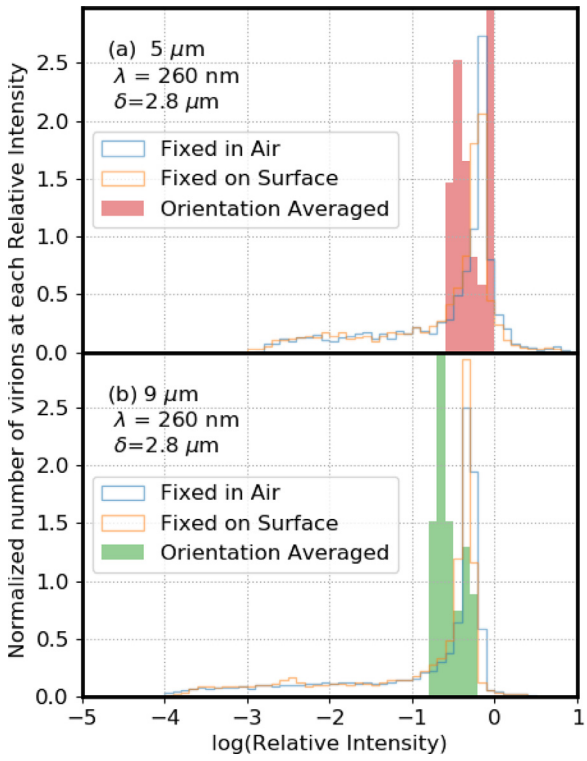

Fig. 7. Relative numbers of virions in bins with the log(relative UV intensities) shown. The distributions in solid bars are for intensities averaged over all orientations. Distributions shown by the blue lines are for the same particle in air, but in a single orientation. Distributions shown by the orange lines are for the same particle, but held on a surface (m_r = 1.4) at a single orientation. In (a) the particle is 5-μm diameter. In (b) the particle is 9-μm diameter. The R_i for the "Orientation Averaged" and "Fixed in Air" are both relative to a single virion in air. The R_i for the "Fixed on Surface" are relative to a single virion on the same surface. The orientation-averaged simulations used in (a) 3000 virions (30 runs of 100 virions for a 9-μm particle), and in (b) 1000 particles (40 runs of 25 virions for a 5-μm particle). The area under the each distribution is normalized to 1.

4.2.4. Dried droplets are neither perfectly spherical nor optically homogeneous

Actual dried particles of airway fluids containing virions are neither perfectly spherical nor optically homogeneous. For particles formed by drying droplets of simulated respiratory fluids (water, mucin, NaCl and DPPC) on a superhydrophobic surface, the particles with sizes similar to those modeled here were somewhat spherical [75]. In the larger dried droplets, crystals of mucin, NaCl, and DPPC formed, in some cases making the particles inhomogeneous and less spherical [75]. The use of four components (NaCl, mucin, DPPC and water) for the simulated saliva may be the reason for this crystallization into what appear to be somewhat pure materials, and the resulting nonsphericity. Human saliva, on the other hand, is more complex [2,11,19,54,55] as seen in Section 2.2 above. There are many different inorganic (Na^+, K^+, Mg^{2+}, Ca^{2+}, Cl^-, PO_4^{3-}, HCO_3^-, SCN^-, F^-) electrolytes, organic acids (lactic and uric acids), glucose, amino acids, peptides, proteins, nucleic acids, etc. Also, DNA and RNA in saliva increase the viscosity. It is therefore not clear which materials, if any, crystalize as pure components when droplets of airway fluids dry, and therefore, whether this possible cause of nonsphericity and inhomogeneity is relevant in dried droplets of actual respiratory fluids.

Although there are uncertainties about the shapes and homogeneities of dried droplets of airway fluids, some general comments about shielding in such particles can be made. First, as illustrated in the first panel of Fig. 1, neither refractive nor absorptive shielding requires spherical particles. Second, given the complexity of airway fluids, it seems unlikely that differences in refractive index within the particle will be as large as those between pure NaCl and a typical pure protein. A small amount of inhomogeneity inside a spherical particle appears to have a small effect on the UV intensities within virions. For example, adding 90 randomly located virions to a 9 μm particle containing 10 virions resulted in changes in R_i of the initial 10 virions ranging from 0.03% to -0.27% (Fig. S1). Third, if the surface of a particle were sufficiently rough that it scattered the UV light in all directions as the light entered the particle, then, as can be envisioned using Fig. 1a and b, refractive shielding could be far less than it would be in an otherwise identical particle with a smooth surface. A nonsphericity that could decrease shielding in particles with a large ratio of penetration depth to particle size, would be a highly inhomogeneous particle with rough surface, where the UV light is scattered in all directions. Fourth, inhomogenities such as large air pockets forming within droplets as they dry, or large cracks occurring as the particles shrink, may have large impacts on the UV intensity distribution. It is, however, difficult to see how a single air pocket or crack would eliminate the potential for refractive shielding, at least at some illumination angles, unless there were multiple cracks and the sides of them were rough. Also, air pockets or wide cracks could decrease absorptive shielding for some illumination angles. Fifth, the locations of the virions in particles are not known [75]. However, it is easy to imagine that as a droplet dries, and as water evaporates and leaves behind a more concentrated region near the droplet surface, the 100-nm virions may be more likely to diffuse more slowly toward center of the droplet (where the concentration of everything except water is lower) than do proteins and smaller molecules. If that is the case, and so if virions are more likely to occur in the outer fraction of the dried droplet, then the fraction of particles which can be refractively shielded is likely to be higher than indicated in the figures and in Table 3. Fig. 2 shows that for a particle on a surface and a normally incident plane wave, the most shielded virions are near the outside of the particle. Even for δ = 2.84 μm and the 9-μm particle (Fig 2b), virions within approximately 2 μm of the center point of the particle appear to have R_i > 0.1. In the outer approximately 1.5 μm of the hemisphere closest to the surface, some particles are well-shielded. Thus, if the virions localize to the surface of the dried droplet as may be plausible, the overall shielding would likely increase for fixed particles on a surface.

4.3. Interventions to circumvent the effects of shielding of virions from UV light

For inactivation of virions in particles on surfaces, the data in Fig 6d-g and Table 3 suggest that multiple UV-light sources positioned to illuminate from widely varying angles can reduce shielding in supermicron particles. Similar reductions in shielding could be obtained using movable light sources. Highly UV reflective paint on walls and surfaces in a room [34,59,60] increase the total UV intensity illuminating particles, and can increase the UV intensities in otherwise shielded regions, partly by increasing the number of directions from which a particle is illuminated.

For inactivation of particles in air, UV illumination of particles from many angles can be easier to achieve because particles can change their orientation with respect to the source(s) of UV illumination as they move through a UVGI system and can spin about an particle or tumble as the axis rotates. However the extent of rotation depends on the particle size, the time it is illuminated, the air flows, and the degree of turbulence. Brownian rotational diffusion decrease with particle size. To reduce the need for rotation of particles about their axis (in order to avoid shielding) UVGI systems that illuminate particles somewhat uniformly from all directions may be ideal. Alternatively, UVGI systems which illuminate from

one direction, or directions separated by a not-large angle, may reduce shielding if they are designed so that even the largest particles have sufficient time to spin and tumble through a sufficiently wide range of angles as they flow through the system (and approximate the all-orientations results of Fig. 7). In flow-through UVGI systems, filters which remove a high percentage of particles larger than, e.g., 5 μm, are common [32]. Such filters reduce the need to design UVGI systems to inactivate larger particles. Rotation of particles in turbulent air flowing through a UVGI or other system is a topic that appears to need further investigation.

5. Conclusions

Virions in particles may be partially shielded from UV. Shielding does not occur in the 0.1 μm naked virions studied here, is small in the 1-μm particles, and increases as particle diameters increase to 5- and 9 μm. Absorptive shielding is more important at the wavelengths of germicidal UV (260 nm used here) than it is at solar UV wavelengths (302 nm used here). Absorptive shielding is especially important in particles with diameters several times larger than the penetration depth. Refractive shielding occurs even in weakly UV-absorbing particles. UV illumination from multiple directions, widely separated, can reduce shielding (Fig. 6d–g). The largest reduction in shielding occurs in particles orientationally averaged with respect to the UV illumination (equivalent to equal illumination from all directions).

The extent to which these modeling results apply to actual dried droplets of respiratory fluids depends on the characteristics of the actual dried particles. Here, the optical properties of the droplets are assumed to be homogeneous (except for the virions), and all droplets and virions are assumed to be spherical. The effects of nonsphericity, inhomogeneous refractive indexes, and the effects of location of the virions are discussed in Section 4.2. As illustrated in Fig. 1a, and readily envisioned from ray optics [9] shielding can occur in nonspherical particles with smooth surfaces.

Key points relevant to designers and users of UVGI systems, or to persons relying on inactivation by solar UVB are as follows. Virions in supermicron particles can be shielded from UV. The extent of shielding increases with particle size (Fig. 3). Shielding tends to be reduced when the UV illumination is from widely separated directions (Fig. 6d–g). The reduction in shielding is greatest when the particles are illuminated equally from all directions (i.e., orientationally averaged) as in Fig. 7. These results suggests that in designing or using UVGI systems on surfaces, shielding could be reduced by using multiple UV sources (or a mobile UV source), or by using highly reflective paints on surfaces such as walls. For UVGI systems for particles in air, these results suggest that the effectiveness of UV for inactivation of larger particles may be increased by the use of illumination times sufficient to allow particles to spin and/or tumble through multiple orientations, and/or by the use of multiple or spatially-extended UV sources.

Some key questions for designs of UVGI systems for flow-through systems for inactivating virions in particles in air are as follows. Are the particles exposed to UV illumination from enough widely separated angles to achieve approximately uniform illumination as they flow through the device? If the UV sources are pulsed, are particles exposed to enough pulses and/or are the sources large enough and/or are the reflectors or multiple sources sufficient to achieve approximately uniform illumination? Do the particles follow trajectories where they change their orientation with respect to the source(s) of UV illumination as they move through the system, and do so even if they spin and/or tumble negligibly around the particle axes? What are the sizes of the largest particles that can pass through the system (including whatever filters are in place)? These questions point to the need for an improved quantitative understanding of particle rotation (spinning and tumbling) as a function of particle size and shape for various airflows and extent of turbulence.

The results point to the importance of measuring and reporting the particle size distributions in studies of transmission of disease, and in studies of inactivation of virions in dried particles of respiratory fluids. Such data could help in understanding the impact shielding might have on the survival of virions in larger dried saliva droplets, could help validate/invalidate this theoretical work, and may help in reducing the transmission of viral and other diseases.

Code availability

Researchers interested in the MSTM codes to calculate the results can email D.W. Mackowski. Those interested in reproducing the calculations to obtain the figures or Table 3 can email D. C. Doughty. Those interested in reproducing the calculations to obtain Tables 1 or 2 can email S. C. Hill.

Declaration of Competing Interest

The authors declare that they have no known competing financial interests or personal relationships that could have appeared to influence the work reported in this paper.

CRediT authorship contribution statement

David C. Doughty: Conceptualization, Methodology, Software, Investigation, Validation, Writing - original draft, Writing - review & editing. **Steven C. Hill:** Conceptualization, Methodology, Software, Investigation, Validation, Writing - original draft, Writing - review & editing. **Daniel W. Mackowski:** Conceptualization, Methodology, Software, Investigation, Validation, Writing - review & editing.

Acknowledgment

The authors acknowledge partial support from the Defense Threat Reduction Agency (DTRA). Hill and Doughty acknowledge funding from the US Army DEVCOM Army Research Laboratory. The authors are thankful to one reviewer for helpful comments, and to Jay Eversole, Jana Kesavan, Frank Handler, Adam Driks (deceased), Clare Voss, Claire Bonial and Stephanie Lukin for helpful discussions.

Supplementary materials

Supplementary material associated with this article can be found, in the online version, at doi:10.1016/j.jqsrt.2020.107489.

References

[1] Anderson DJ, Moehring RW, Weber DJ, Lewis SS, Chen LF, Schwab JC, Becherer P, Blocker M, Triplett PF, Knelson LP, Lokhnygina Y, Rutala WA, Sexton DJCDC Prevention Epicenters Program. Effectiveness of targeted enhanced terminal room disinfection on hospital-wide acquisition and infection with multidrug-resistant organisms and Clostridium difficile: a secondary analysis of a multicentre cluster randomized controlled trial with crossover design (BETR disinfection). Lancet Infect Dis 2018;18(8):845–53. doi:10.1016/S1473-3099(18)30278-0.

[2] Araujo DS, Scudine KGO, Pedroni-Pereira A, Gaviao MBD, Pereira EC, Fonseca FLA, Castelo PM. Salivary uric acid is a predictive marker of body fat percentage in adolescents. Nutr Res 2020;74:62–70. doi:10.1016/j.nutres.2019.11.007.

[3] Asadi S, Wexler AS, Cappa CD, Barreda S, Bouvier NM, Ristenpart WD. Aerosol emission and superemission during human speech increase with voice loudness. Sci Rep 2019;9(2348):1–9. doi:10.1038/s41598-019-38808-z.

[4] Bang J-I, Park J, Choi A, Jeong J-W, Kim JY, Sung M. Evaluation of UR-UVGI system for sterilization effect on microorganism contamination in negative pressure isolation ward. Sustainability 2018;10:3192. doi:10.3390/su10093192.

[5] Beggs CB, Avital EJ. Upper-room ultraviolet air disinfection might help to reduce COVID-19 transmission in buildings: a feasibility study. PeerJ 2020;8:e10196. doi:10.7717/peerj.10196.
[6] Ben-aryeh H, Shalev A, Szargel R, Laor A, Laufer D, Gutman D. The salivary flow rate and composition of whole and parotid resting and stimulated saliva in young and old healthy subjects. Biochem Med Metab Biol 1986;36:260–5. doi:10.1016/0885-4505(86)90134-9.
[7] Bourouiba L. Turbulent gas clouds and respiratory pathogen emissions potential implications for reducing transmission of COVID-19. JAMA 2020;323:1837–8. doi:10.1001/jama.2020.4756.
[8] Chia PY, et al. Detection of air and surface contamination by SARS-CoV-2 in hospital rooms of infected patients. Nat Commun 2020;11:2800. doi:10.1038/s41467-020-16670-2.rg/10.1038/s41467-020-16670-2.
[9] Chowdhury DQ, Barber PW, Hill SC. Energy-density distribution inside large non-absorbing spheres by using Mie theory and geometrical optics. Appl Opt 1992;31(18):3518–23. doi:10.1364/AO.31.003518.
[10] Duguid JP. The size and duration of air-carriage of respiratory droplets and droplet-nuclei. J Hyg 1946;44(6):471–9. doi:10.1017/s0022172400019288.
[11] Edgar M, Dawes C, O'Mullane D. Saliva and oral health. 4th ed. Stephen Hancocks, Ltd.; 2012. Table 1.2 and references therein, and Fig. 5.4.
[12] Fisher EM, Richardson AW, Harpest SD, Horacre KC, Shaffer RE. Reaerosolization of MS_2 bacteriophage from an N_{95} filtering facepiece respirator by simulated coughing. Ann Occup Hyg 2012;56(3):315–25. doi:10.1093/annhyg/mer101.
[13] Fuchs NA. The mechanics of aerosols. Oxford, England: Pergamon; 1964.
[14] Garcia de Abajo FJ, Hernandez RJ, Kaminer I, Meyerhans A, Rosell-Llompart J, Sanchez-Elsner T. Back to normal: an old physics route to reduce SARS-CoV-2 transmission in indoor spaces. ACS Nano 2020;14:7704–13. doi:10.1021/acsnano.0c04596.
[15] Girardin G, Renault P, Bon F, Capowiez L, Chadoeuf J, Krawczyk C, Courault D. Viruses carried to soil by irrigation can be aerosolized later during windy spells. Agron Sustain Dev 2016;36(59). doi:10.1007/s13593-016-0393-7.
[16] Hakim H, Gilliam C, Tang L, Xu J, Lee L. Effect of a shielded continuous ultraviolet-C air disinfection device on reduction of air and surface microbial contamination in a pediatric oncology outpatient care unit. Am J Infect Control 2019;47:1248–54. doi:10.1016/j.ajic.2019.03.026.
[17] Han ZY, Weng WG, Huang QY. Characterizations of particle size distribution of the droplets exhaled by sneeze. J R Soc Interface 2013;10:20130560. doi:10.1098/rsif.2013.0560.
[18] Handler FA, Edmonds JM. Quantitative analysis of effects of UV exposure and spore cluster size on deposition and inhalation hazards of Bacillus spores. Aerosol Sci Tech 2015;49:1121–30. doi:10.1080/02786826.2015.1102857.
[19] Hawkins GR, Zipkin I, Marshall LM. Determination of uric acid, tyrosine, tryptophan, and protein in whole human parotid saliva by ultraviolet absorption spectrophotometry. J Dent Res 1963;42(4):1015–22. doi:10.1177/00220345630420040301.
[20] Hessling M, Hones K, Vatter P, Lingenfelder C. Ultraviolet irradiation doses for coronavirus inactivation–review and analysis of coronavirus photoinactivation studies. GMS Hyg Infect Control 2020;15 Doc08. doi:10.3205/dgkh000343.
[21] Hill SC, Barnes MD, Lermer N, Whitten WB, Ramsey JM. Simulation of single-molecule photocount statistics in microdroplets. Anal Chem 1998;70:2964–71. doi:10.1021/ac971319d.
[22] Hill SC, Doughty DC, Pan Y-L, Williamson C, Santarpia JL, Hill HH. Fluorescence of bioaerosols: mathematical model including primary fluorescing and absorbing molecules in bacteria: errata. Opt Express 2014;22(19):22817–19. doi:10.1364/OE.22.022817.
[23] Hill SC, Pan YL, Williamson C, Santarpia JL, Hill HH. Fluorescence of bioaerosols: mathematical model including primary fluorescing and absorbing molecules in bacteria. Opt Express 2013;21:22285–313. doi:10.1364/OE.21.022285.
[24] Hill SC, Williamson CC, Doughty DC, Pan Y-L, Santarpia JL, Hill HH. Size-dependent fluorescence of bioaerosols: mathematical model using fluorescing and absorbing molecules in bacteria. J Quant Spectrosc Radiat Transf 2015;157:54–70. doi:10.1016/j.jqsrt.2015.01.011.
[25] IUPAC Compendium of chemical terminology gold book–version 2.3.3. International Union of Pure and Applied Chemistry; 2014. doi:101351/goldbook.
[26] Johnson D, Lynch R, Marshall C, Mead K, Hirst D. Aerosol generation by modern flush toilets. Aerosol Sci Tech 2013;47:1047–57. doi:10.1080/02786826.2013.814911.
[27] Joung YS, Ge Z, Buie CR. Bioaerosol generation by raindrops on soil. Nat Commun 2017;8:14668. doi:10.1038/ncomms14668.
[28] Khare P, Marr LC. Simulation of vertical concentration gradient of influenza viruses in dust resuspended by walking. Indoor Air 2015;25:428–40. doi:10.1111/ina.12156.
[29] Kesavan JS, Humphreys PD, Bottiger JR, Valdes ER, Rastogi VK, Knox CK. Deposition method, relative humidity, and surface property effects of bacterial spore reaerosolization via pulsed air jet. Aerosol Sci Tech 2017;51(4):1027–34. doi:10.1080/02786826.2017.1335389.
[30] Kesavan J, Schepers D, Bottiger J, Edmonds J. UV-C decontamination of aerosolized and surface-bound single spores and bioclusters. Aerosol Sci Tech 2014;48:450–7. doi:10.1080/02786826.2014.889276.
[31] Kim D-K, Kang D-H. UVC LED irradiation effectively inactivates aerosolized viruses, bacteria, and fungi in a chamber-type air disinfection system. Appl Environ Microbiol 2018;84 e00944-18. doi:10.1128/AEM.00944-18.
[32] Kowalski W. Ultraviolet germicidal irradiation handbook: UVGI for air and surface disinfection. New York: Springer; 2009. doi:101007/978-3-642-01999-9.
[33] Krauter P, Biermann A. Reaerosolization of fluidized spores in ventilation systems. Appl Environ Microbiol 2007;73(7):2165–72. doi:10.1128/AEM.02289-06.
[34] Krishnamoorthy G, Tande BM. Improving the effectiveness of ultraviolet germicidal irradiation through reflective wall coatings: experimental and modeling based assessments. Indoor Built Environ 2016;25:314–28. doi:10.1177/1420326X14547785.
[35] Kujundzic E, Hernandez M, Miller SL. Ultraviolet germicidal irradiation inactivation of airborne fungal spores and bacteria in upper-room air and HVAC in-duct configurations. J Environ Eng Sci 2007;6:1–9. doi:10.1139/s06-039.
[36] Layshock JA, Pearson B, Crockett K, Brown MJ, Van Cuyk S, Daniel WB, Omberg KM. Reaerosolization of Bacillus spp. in outdoor environments: a review of the experimental literature. Biosecur Bioterror 2012;10(3):299–303. doi:10.1089/bsp.2012.0026.
[37] Leung NHL, Chu DKW, Shiu EYC, Chan K-H, McDevitt JJ, Hau BJP, Yen H-L, Li Y, Ip DKM, Peiris JSM, Seto W-H, Leung GM, Milton DK, Cowling BJ. Respiratory virus shedding in exhaled breath and efficacy of face masks. Nat.Med 2020;26:676–80. doi:10.1038/s41591-020-0843-2.
[38] Li Y, Wang J-X, Chen X. Can a toilet promote virus transmission? From a fluid dynamics perspective. Phys Fluids 2020;32:065107. doi:10.1063/5.0013318.
[39] Liu Y, et al. Aerodynamic analysis of SARS-CoV-2 in two Wuhan hospitals. Nature 2020;582:557–60. doi:10.1038/s41586-020-2271-3.
[40] Lighthart B, Shaffer BT, Marthi B, Ganio LM. Artificial wind-gust liberation of microbial bioaerosols previously deposited on plants. Aerobiologia 1993;9:189–96. doi:10.1007/BF02066261.
[41] Mackowski DW. Exact solution for the scattering and absorption properties of sphere clusters on a plane surface. J Quant Spectrosc Radiat Transf 2008;109:770–88. doi:10.1016/j.jqsrt.2007.08.024.
[42] Mackowski DW, Mishchenko MI. Calculation of the T matrix and the scattering matrix for ensembles of spheres. 1996. J Opt Soc Am A 1996;13(11):2266–78. doi:10.1364/JOSAA.13.002266.
[43] Mackowski DW, Mishchenko MI. A multiple sphere T-matrix Fortran code for use on parallel computer clusters. J Quant Spectrosc Radiat Transf 2011;112:2182–92. doi:10.1016/j.jqsrt.2011.02.019.
[44] Mackowski DW, Mishchenko MI. Direct simulation of extinction in a slab of spherical particles. J Quant Spectrosc Radiat Transf 2013;109:770–88. doi:10.1016/j.jqsrt.2013.02.008.
[45] Marr LC, Tang JW, Van Mullekom J, Lakdawala SS. Mechanistic insights into the effect of humidity on airborne influenza virus survival, transmission and incidence. J R Soc Interface 2019;16:20180298. doi:10.1098/rsif.2018.0298.
[46] Memarzadeh F, Olmsted RN, Bartley JM. Applications of ultraviolet germicidal irradiation disinfection in health care facilities: effective adjunct, but not stand-alone technology. Am J Infect Control 2010;38:S13–24. doi:10.1016/j.ajic.2010.04.208.
[47] Milton DK, Fabian MP, Cowling BJ, Grantham ML, McDevitt JJ. Influenza virus aerosols in human exhaled breath: particle size, culturability, and effect of surgical masks. PLoS Pathog 2013;9(3):e1003205. doi:10.1371/journal.ppat.1003205.
[48] Morawska L, Johnson GR, Ristovski ZD, Hargreaves M, Mengersen K, Corbett S, Chao CYH, Li Y, Katoshevski D. Size distribution and sites of origin of droplets expelled from the human respiratory tract during expiratory activities. J Aerosol Sci 2009;40:256–69. doi:10.1016/j.jaerosci.2008.11.002.
[49] Morawska L, Milton DK. It is time to address airborne transmission of COVID-19. Clin Infect Dis 2020 ciaa939. doi:10.1093/cid/ciaa939.
[50] Nardell EA, Nathdvitharana RR. Airborne spread of SARS-CoV-2 and a potential role for air disinfection. JAMA 2020;324(2):141–2. doi:10.1001/jama.2020.7603.
[51] Osman S, Peeters Z, La Duc MT, Mancinelli R, Ehrenfreund P, Venkateswaran K. Effect of shadowing on survival of bacteria under conditions simulating the Martian atmosphere and UV radiation. Appl Environ Microbiol 2008;74(4):959–70. doi:10.1128/AEM.01973-07.
[52] Park SY, Kim A-N, Lee K-H, Ha S-D. Ultraviolet-C efficacy against a norovirus surrogate and hepatitis A virus on a stainless steel surface. Int J Food Microbiol 2015;211:73–8. doi:10.1016/j.ijfoodmicro.2015.07.006.
[53] Paton S, Thompson K-A, Parks SR, Bennett AM. Reaerosolization of spores from flooring surfaces to assess the risk of dissemination and transmission of infections. Appl Environ Microbiol 2015;81(15):4914–19. doi:10.1128/AEM.00412-15.
[54] Peden DB, Hohman R, Brown ME, Mason RT, Berkebile C, Fales HM, Kaliner MA. Uric acid is a major antioxidant in human nasal airway secretions. PNAS 1990;87:7638–42. doi:10.1073/pnas.87.19.7638.
[55] Poehls UG, Hack CC, Ekici AB, Beckmann MW, Fasching PA, Ruebner M, Huebner H. Saliva samples as a source of DNA for high throughput genotyping: an acceptable and sufficient means in improvement of risk estimation throughout mammographic diagnostics. Eur J Med Res 2018;23(20). doi:10.1186/s40001-018-0318-9.
[56] Prussin AJ, Marr LC. Sources of microorganisms in the built environment. Microbiome 2015;3:78. doi:10.1186/s40168-015-0144-z.
[57] Qian J, Peccia J, Ferro AR. Walking-induced particle resuspension in indoor environments. Atmos Environ 2014;89:464–81. doi:10.1016/j.atmosenv.2014.02.035.
[58] Ratnesar-Shumate S, Williams G, Green B, et al. Simulated sunlight rapidly inactivates SARS-CoV-2 on surfaces. J Infect Dis 2020. doi:10.1093/infdis/jiaa274.

[59] Rutala WA, Gergen MF, Tande BM, Weber DJ. Rapid hospital room decontamination using ultraviolet (UV) light with a nanostructured UV-reflective wall coating. Infect Cont Hosp Ep 2013;34:527–9. doi:10.1086/67021.
[60] Ryan K, McCabe K, Clements N, Hernandez M, Miller SL. Inactivation of airborne microorganisms using novel ultraviolet radiation sources in reflective flow-through control devices. Aerosol Sci Technol 2010;44:541–50. doi:10.1080/02786821003762411.
[61] Sagripanti J-L, Lytle CD. Inactivation of influenza virus by solar radiation. Photochem Photobiol 2007;83:1278–82. doi:10.1111/j.1751-1097.2007.00177.x.
[62] Sagripanti J-L, Lytle CD. Sensitivity to ultraviolet radiation of Lassa, vaccinia, and Ebola viruses dried on surfaces. Arch Virol 2011;156:489–94. doi:10.1007/s00705-010-0847-1.
[63] Sagripanti J-L, Voss L, Marschall H-J, Lytle CD. Inactivation of vaccinia virus by natural sunlight and by artificial UVB radiation. Photochem Photobiol 2013;89:132–8. doi:10.1111/j.1751-1097.2012.01207.x.
[64] Sagripanti J-L, Lytle CD. Estimated inactivation of coronaviruses by solar radiation with special reference to COVID-19. Photochem Photobiol 2020. doi:10.1111/php.13293.
[65] Sagripanti J-L, Rom AM, Holland LE. Persistence in darkness of virulent alphaviruses, Ebola virus, and Lassa virus deposited on solid surfaces. Arch Virol 2010;155:2035–9. doi:10.1007/s00705-010-0791-0.
[66] Santarpia J.L., Herrera V.L., Rivera D.N., Ratnesar-Shumate S., Reid S.P., Denton P.W., Martens J.W.S., Fang Y., Conoan N., Callahan M.V., Lawler J.V., Brett-Major D.M., Lowe, J.J. The infectious nature of patient-generated SARS-CoV-2 aerosol. 2020; mdRXiv preprint doi:10.1101/2020.07.13.20041632.
[67] Schuit M, Gardner S, Wood S, Bower K, Williams G, Freeburger D, Dabisch P. The influence of simulated sunlight on the inactivation of influenza virus in aerosols. J Infect Dis 2020;221:372–8. doi:10.1093/infdis/jiz582.
[68] Simmons SE, Carrion R, Alfson KJ Jr., Staples HM, Jinadatha C, Jarvis WR, Sampathkumar P, Chemaly RF, Khawaja F, Povroznik M, Jackson S, Kaye KS, Rodriguez RM, Stibich MA. Deactivation of SARS-CoV-2 with pulsed-xenon ultraviolet light: Implications for environmental COVID-19 control. Infect Control Hosp Epidemiol 2020:1–4. doi:10.1017/ice.2020.399.
[69] Sirotkin VA, Komissarov IA, Khadiullina AV. Hydration of proteins: excess partial volumes of water and proteins. J Phys Chem 2012;116:4098–105. doi:10.1021/jp300726p.
[70] Spencer RC. Bacillus anthracis. J Clin Pathol 2003;56:182–7.
[71] Tseng C-C, Li C-S. Inactivation of viruses on surfaces by ultraviolet germicidal irradiation. J Occup Environ Hyg 2007;4(6):400–5. doi:10.1080/15459620701329012.
[72] van Doremalen N, Bushmaker T, Morris DH, Holbrook MG, Gamble A, Williamson BN, Tamin A, Harcourt JL, Thornburg NJ, Gerber SI, Lloyd-Smith JO, de Wit E, Munster VJ. Aerosol and surface stability of SARS-CoV-2 as compared with SARS-CoV-1. N Engl J Med 2020;382:1564–7. doi:10.1056/NEJMc2004973.
[73] van Nieuw Amerongen A, Bolscher JGM, Veerman ECI. Salivary proteins: protective and diagnostic value in cariology? Caries Res 2004;38:247–53. doi:10.1159/000077762.
[74] Veerman ECI, van den Keybus PAM, Vissink A, Nieuw Amerongen AV. Human glandular salivas: their separate collection and analysis. Eur J Oral Sci 1996;104:346–52. doi:10.1111/j.1600-0722.1996.tb00090.x.
[75] Vejerano EP, Marr LC. Physico-chemical characteristics of evaporating respiratory fluid droplets. J R Soc Interface 2018;15(139):20170939 0939. doi:10.1098/rsif.2017.0939.
[76] Walker CM, Ko GW. Effect of ultraviolet germicidal irradiation on viral aerosols. Env Sci Technol 2007;41(15):5460–5. doi:10.1021/es070056u.
[77] Woo M-H, Grippin A, Anwar D, Smith T, Wu C-Y, Wander JD. Effects of relative humidity and spraying medium on UV decontamination of filters loaded with viral aerosols. Appl Environ Microbiol 2012;78(16):5781–7. doi:10.1128/AEM.00465-12.
[78] Wyllie AL, Fournier J, Casanovas-Massana A, et al. Saliva or nasopharyngeal swab specimens for detection of SARS-CoV-2. N Engl J Med 2020;383:1283–6 2020. doi:10.1056/NEJMc2016359.